Ovarian cancer progression is controlled by phenotypic changes in dendritic cells

Uciane K. Scarlett,[1] Melanie R. Rutkowski,[1] Adam M. Rauwerdink,[2] Jennifer Fields,[3] Ximena Escovar-Fadul,[1] Jason Baird,[4] Juan R. Cubillos-Ruiz,[4] Ana C. Jacobs,[4] Jorge L. Gonzalez,[5] John Weaver,[2] Steven Fiering,[3,4] and Jose R. Conejo-Garcia[1]

[1]Immunology Program, the Wistar Institute, Philadelphia, PA 19104
[2]Department of Radiology, [3]Department of Genetics, [4]Department of Microbiology and Immunology, and [5]Department of Pathology, Dartmouth Medical School, Lebanon, NH 03756

We characterized the initiation and evolution of the immune response against a new inducible p53-dependent model of aggressive ovarian carcinoma that recapitulates the leukocyte infiltrates and cytokine milieu of advanced human tumors. Unlike other models that initiate tumors before the development of a mature immune system, we detect measurable anti-tumor immunity from very early stages, which is driven by infiltrating dendritic cells (DCs) and prevents steady tumor growth for prolonged periods. Coinciding with a phenotypic switch in expanding DC infiltrates, tumors aggressively progress to terminal disease in a comparatively short time. Notably, tumor cells remain immunogenic at advanced stages, but anti-tumor T cells become less responsive, whereas their enduring activity is abrogated by different microenvironmental immunosuppressive DCs. Correspondingly, depleting DCs early in the disease course accelerates tumor expansion, but DC depletion at advanced stages significantly delays aggressive malignant progression. Our results indicate that phenotypically divergent DCs drive both immunosurveillance and accelerated malignant growth. We provide experimental support for the cancer immunoediting hypothesis, but we also show that aggressive cancer progression after a comparatively long latency period is primarily driven by the mobilization of immunosuppressive microenvironmental leukocytes, rather than loss of tumor immunogenicity.

CORRESPONDENCE
Jose R. Conejo-Garcia:
jrconejo@wistar.org

Abbreviations used: DLN, draining LN; IOSE, immortalized ovarian surface epithelial.

Epithelial ovarian cancer is a devastating disease responsible for the deaths of ~15,000 Americans per year, even more than melanoma or brain tumors (Jemal et al., 2009). Independent studies have demonstrated that in the ovarian carcinoma microenvironment, T cells (and only they) can spontaneously exert clinically relevant pressure against tumor progression (Zhang et al., 2003; Sato et al., 2005; Hamanishi et al., 2007). However, as the dismal statistics show, immune pressure against established tumors is insufficient. In part, this is because when tumors become clinically symptomatic, they have already overcome the immune system through multiple complementary mechanisms. The "cancer immunoediting" hypothesis, supported by recent experimental and clinical evidence, provides a frame to understand this process (Schreiber et al., 2011). The model implies that all symptomatic tumors represent a failure of the immune system. Recent studies have postulated that tumors can be kept in check for long periods, through a dynamic balance that results in the progressive loss of immunogenicity by tumor cells. However, emerging clinical evidence from multiple trials blocking common immunosuppressive checkpoints (such as CTLA4 or PD-1) indicates that preventing tumor-induced T cell paralysis restores protective immunity against established cancers, implying that advanced tumors remain somewhat immunogenic. Based on multiple lines of evidence, the model has recently evolved to include the role of immunosuppression in the tumor microenvironment in this process. However, the relative contribution of individual microenvironmental populations to suppress or support the capacity of tumors to expand and their dynamics remains unclear.

The Rockefeller University Press $30.00
J. Exp. Med. Vol. 209 No. 3 495-506
www.jem.org/cgi/doi/10.1084/jem.20111413

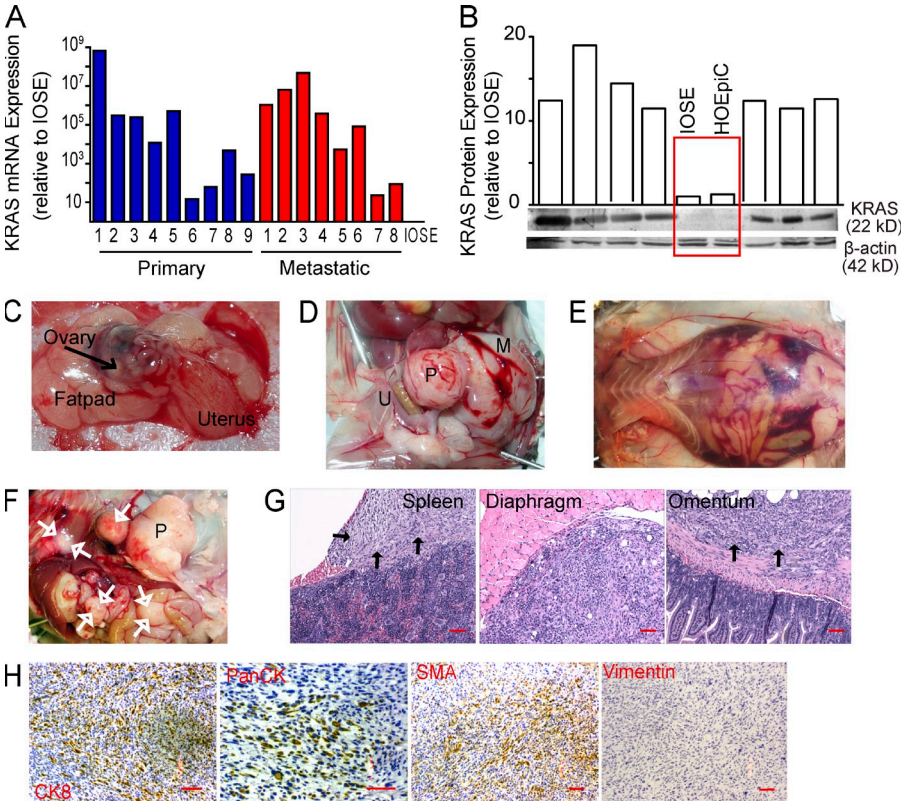

Figure 1. The p53-dependent mouse model of ovarian carcinoma develops solid peritoneal tumor masses. (A) Expression of *KRAS* mRNA (normalized to *GAPDH*) in 17 representative cases of stage III–IV human ovarian carcinomas, relative to IOSE cells (immortalized cells from the normal ovarian epithelial surface). (B) Relative protein expression of K-ras (normalized to β-actin) in seven randomly selected stage III–IV human ovarian carcinoma specimens, IOSE cells, or HOSEpiC cells (healthy ovarian epithelial cells cryopreserved either at primary or passage one cultures). (C) Injection of trypan blue into the bursal cavity of transgenic mice. (D) Intrabursal adenoviral injection in p53/K-ras mice results in a primary solid ovarian tumor mass (*P*) with accompanying metastatic lesion (*M*). *U*, uterus. (E) Ascites detected in the peritoneal cavity of a chimeric p53/K-ras mouse injected with the adenovirus ∼50 d before. (F) Primary (*P*) and spontaneous metastatic masses (white arrows) in p53/K-ras mice 50 d after receiving adenovirus. (G) H&E of metastatic masses from indicated regions which appeared in mice 3 mo after undergoing resection of primary tumors at ∼35 d. Black arrows indicate tumor tissue. Bars, 100 µm. (H) p53/K-ras primary epithelial tumors stained for Cytokeratin 8 (CK8; ×100), Pan-Cytokeratin (PanCK; ×200), smooth muscle actin (SMA; ×100); and Vimentin (×100). Bars, 100 µm. Brightness, contrast, and color balance were uniformly adjusted in whole individual images.

Some excellent non-transplantable models of ovarian cancer are available, but mutagenic events activated during embryonic development result in animals that are born with premalignant lesions (Connolly et al., 2003; Xing et al., 2009), which complicates their use for understanding tumor initiation. For instance, seminal studies by Clark et al. (2007), using a genetic model of pancreatic cancer, found immune tolerance against cancer soon after birth. This may reflect the distinctive physiopathology of pancreatic cancer but also be the result of defective immunosurveillance when mutations are initiated before the development of a mature immune system.

To understand how the evolution of the inflammatory microenvironment of developing aggressive ovarian cancers influences tumor progression, we have generated a new p53-dependent model that recapitulates the immune populations of human tumors in previously healthy hosts. Our results show that accelerated malignant progression after a relatively long period of immune control is triggered by a phenotypic switch in expanding DC infiltrates, which can be reversed upon DC depletion, without specifically ablating tumor cells.

RESULTS

Generation of a p53-dependent inducible metastatic ovarian carcinoma

To model the immunobiology of aggressive (type II) ovarian cancers (Kurman and Shih, 2011), we first sought to generate an inducible cancer model in previously healthy adult mice, avoiding the initiation of carcinogenic events before the development of a mature immune system. For that purpose, we used a previously described technique (Flesken-Nikitin et al., 2003; Dinulescu et al., 2005), based on the delivery of recombinant adenoviruses expressing Cre recombinase into the ovarian bursal cavity. Ablation of only p53—the hallmark of malignancy in human ovarian carcinoma (Bernardini et al., 2010)—did not result in any obvious carcinogenic event >200 d after induction of the mutation (not depicted). To add a relevant second mutagenic event, we investigated the occurrence of *KRAS* deregulation in a cohort of 60 unselected stage III–IV human ovarian carcinoma specimens. We found highly variable levels of KRAS mRNA in both metastatic and primary specimens, but all were higher than the very low levels of an immortalized ovarian surface epithelial (IOSE) cell line (Wang et al., 2006; Fig. 1 A). Most importantly, KRAS protein was also dramatically overexpressed in multiple tumors, compared with IOSE cells or HOSEpiC epithelial cells from healthy ovaries cryopreserved either at primary or passage one cultures (Fig. 1 B), indicating that, beyond the frequent gene amplification recently reported by the Cancer Genome Atlas Network (Bell et al., 2011), KRAS is deregulated in most advanced human ovarian cancers.

To model the constitutive activation of KRAS, we took advantage of existing LSL-K-ras$^{G12D/+}$ mice (Jackson et al., 2001). Intrabursal delivery makes injected materials accessible to both the epithelial surface and the fimbriated epithelium at the interphase with the oviduct (Fig. 1 C). Concurrent ablation of p53 and activation of oncogenic K-ras in double (p53/K-ras)

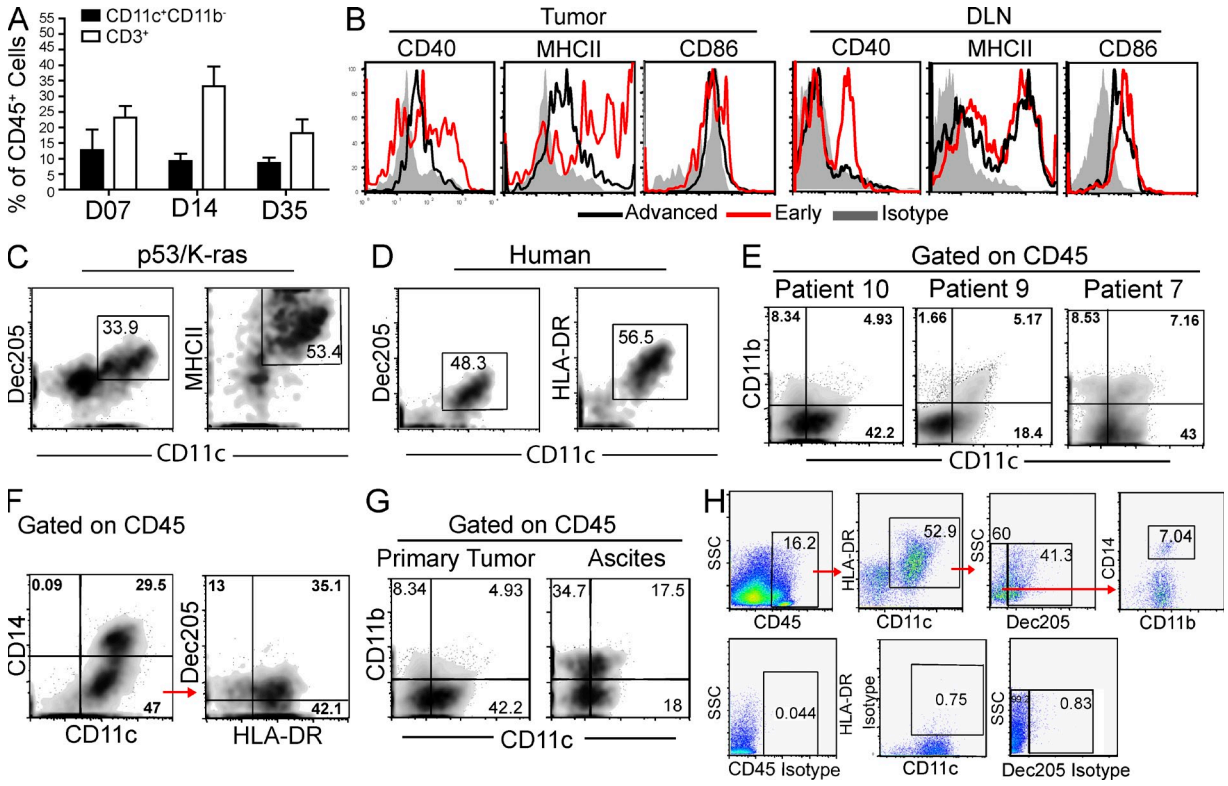

Figure 2. The inflammatory microenvironment of p53/K-ras end-stage tumors recapitulates advanced human ovarian carcinoma. (A) Quantification at the indicated time points of cells found within the ovaries of WT animals ($n = 8$) after receiving adenovirus intrabursally. Gated on CD45+ cells. (B) Expression of indicated activation markers on CD45+CD11c+ DCs taken from tumors or DLN of p53/K-ras mice. Early, 7 d after AdvCre injection; Advanced, mice with advanced tumors. Representative density plots of dissociated tumors from p53/K-ras mice (C) and patients with stage III–IV ovarian carcinoma (gated on CD45; D). (E–G) Density flow plots of dissociated tumors from individual patients with stage III–IV ovarian carcinoma. (H) Gating strategy (above) and isotypes (below) for Table 1. Error bars, SEM.

transgenic mice then resulted in palpable abdominal tumor lesions with 100% penetrance only 35 d after adenoviral administration. Tumors were found to be perfectly solid as they became more advanced (Fig. 1 D). In a proportion of animals we detected gross hemorrhagic ascites (Fig. 1 E), as well as metastases at multiple peritoneal locations (Fig. 1, F and G).

Histological sections of the primary and metastatic tumor sites revealed a growth pattern characterized by solid masses comprised of malignant spindled cells with interspersed large anaplastic tumor cells. The neoplastic cells were immunoreactive for cytokeratin 8, desmin (not depicted), and smooth muscle actin and were negative for vimentin (Fig. 1 H). Patchy immunoreactivity with a pan-cytokeratin antibody cocktail was also noted (Fig. 1 H). Although on a morphological basis, sarcoma is a consideration, the immunohistochemical staining pattern is most consistent with sarcomatoid ovarian carcinoma (i.e., induction of a high-grade poorly differentiated ovarian carcinoma with spindle cell morphology). Together, these data indicate that concurrent p53 and K-ras mutations in the epithelial ovarian surface and/or fimbriated epithelium at the interphase with the oviduct result in highly metastatic tumors with complete penetrance and short latency.

Inducible ovarian tumors recapitulate the inflammatory microenvironment of human ovarian cancer

Nonreplicating adenoviral-Cre delivery in WT mice altered the leukocytic ovarian microenvironment only in a temporary manner, as the proportions of tissue-resident CD11c+ DCs were unchanged between 1 and 5 wk after surgical manipulation (Fig. 2 A). Ovarian T cell infiltration (the other predominant leukocyte subset in healthy ovaries) was similarly unaffected (Fig. 2 A). However, when we performed an exhaustive phenotypic analysis of the immune microenvironment of solid advanced p53/K-ras tumor masses, we found a relatively homogeneous population of CD11c+DEC205+MHC-II+ CD11b+CD86−CD40low DCs, supporting our previous observations in transplantable models (Scarlett et al., 2009; Fig. 2, B and C). These populations of DCs expressing low levels of co-stimulatory molecules were also present in tumor draining LNs (DLNs) of animals with end stage tumors (Fig. 2 B). Most importantly, terminal tumors recapitulated the immune microenvironment of advanced human ovarian carcinomas, including a heterogeneous mix of antigen-presenting cells (Wilke et al., 2011). Thus, in advanced solid tumors of humans and p53/K-ras mice, the predominant leukocyte subset expressed phenotypic markers of bona fide DCs, including

Table 1. Flow analysis of leukocytes infiltrating solid Stage III/IV human ovarian tumors

Patients	Gated on CD45		Gated on CD11c⁺HLA-DR⁺		Gated on Dec205⁻	Gated on CD45	
	CD11c⁺	CD11c⁺HLA-DR⁺	Dec205⁺	Dec205⁻	CD11b⁺CD14⁺	CD20⁺	CD3⁺
S1 Patient 1	52	30.9	39.9	61.7	28.6	1.78	30.9
S2 Patient 2	47.2	47.1	59.1	39.4	29.2	2.79	45.7
S4 Patient 3 (*P*)	84.7	82.2	17.2	81.2	4.9	n/a	n/a
S5 Patient 3 (*M*)	84.8	56.3	12	76.8	15.6	n/a	n/a
S6 Patient 4	12	12.3	70.3	30.1	44.5	n/a	n/a
S7 Patient 5	57.1	56.5	70.3	25.8	21.5	n/a	n/a
S8 Patient 6	52.8	52.4	41.3	59.9	7.04	1.78	30.9
S9 Patient 7	41.7	40	n/a	n/a	n/a	0.27	10.2
S10 Patient 8	28.2	6.35	n/a	n/a	n/a	0.013	0.49
S11 Patient 9	37.2	36.5	n/a	n/a	n/a	2.85	8.34
S12 Patient 10	37.1	5.4	n/a	n/a	n/a	0.045	1.92

Gating strategy is outlined in Fig. 2 H. n/a, insufficient material. Values are expressed as percentages.

CD11c, DEC205, and MHC-II (Fig. 2, C and D). In humans, the precise categorization of solid tumor-infiltrating myeloid leukocytes was more complicated as the result of a high degree of phenotypic overlap between DCs and macrophages in some specimens. However, the most abundant leukocyte in at least a third of the specimens analyzed clearly lacked the monocyte/macrophage markers CD11b or CD14 but coexpressed the DC marker CD11c (Fig. 2, E–G; and Table 1). These cells also maintain a high level of expression of MHC-II, so they cannot be alternatively defined as more immature myeloid-derived suppressor cells (Nagaraj and Gabrilovich, 2010; Fig. 2 H and Table 1). Interestingly, DCs in our mouse model progressively down-regulated MHC-II expression until ∼35 d, whereas DCs found within advanced tumors (>50 d) showed intermediate MHC-II expression. In contrast, the microenvironment of ascites showed the presence of predominant bona fide macrophages (Fig. 2 G). Therefore, the distinctive product of excessive myelopoiesis in most human ovarian cancer solid tumor masses is a leukocyte with predominant phenotypic attributes of DCs, rather than canonical macrophages, which is recapitulated in our animal model.

Besides corresponding expression of phenotypic determinants, CD45⁺CD11c⁺MHC-II⁺ DCs sorted from dissociated p53/K-ras advanced tumors and CD45⁺CD11c^{hi}HLA-DR^{hi}-Dec205^{int} from unselected human tumor specimens responded to PMA and ionomycin by secreting a comparable pattern of proinflammatory chemokines. Those included high levels of CCL3 and CCL4, in addition to pro-angiogenic IL-8/KC (Fig. 3 A). A similar cytokine profile was found in DCs sorted from a transplantable mouse model of ovarian cancer (ID8-*Defb29/Vegf-A*; Fig. 3 A). Together, these data indicate that our p53-dependent tumor model faithfully recapitulates the immune microenvironment of human ovarian cancer, and it is therefore suitable to understand its unknown dynamics.

Accelerated tumor growth after prolonged stability coincides with a switch in the inflammatory infiltrate

We found that, starting after day 21 after the adenovirus-Cre challenge, tumors accumulated progressively denser immune cell infiltrates (Fig. 3, B and C). Remarkably, tumor progressed through a prolonged equilibrium phase for ∼28 d, when no obvious macroscopic masses were detectable (Fig. 4 A, top). Leukocytes other than DCs in tumor-developing ovaries at

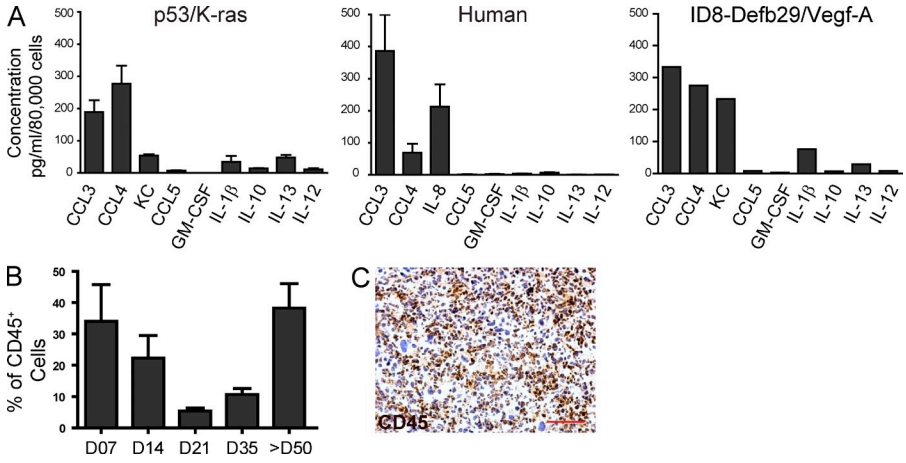

Figure 3. DCs found within solid p53/K-ras tumors display similar proinflammatory attributes as human tumor-derived DCs. (A) Quantification of cytokines and chemokines secreted from sorted CD45⁺CD11c⁺Dec205⁺CD11b$^{+/-}$ cells from advanced human tumor specimens (n = 3) or CD45⁺CD11c⁺CD11b⁺ cells from tumors of end-stage p53/K-ras mice (n = 4) or ascites of WT mice bearing ID8-*Defb29/Vegf-a* tumors. (B) Proportion of CD45⁺ cells found within the ovaries of p53/K-ras mice (n = 6) at the indicated time points after adenovirus injection. (C) CD45 immunohistochemical analysis of resected tumors (>50 d) ×100. Error bars, SEM. Bar, 100 µm.

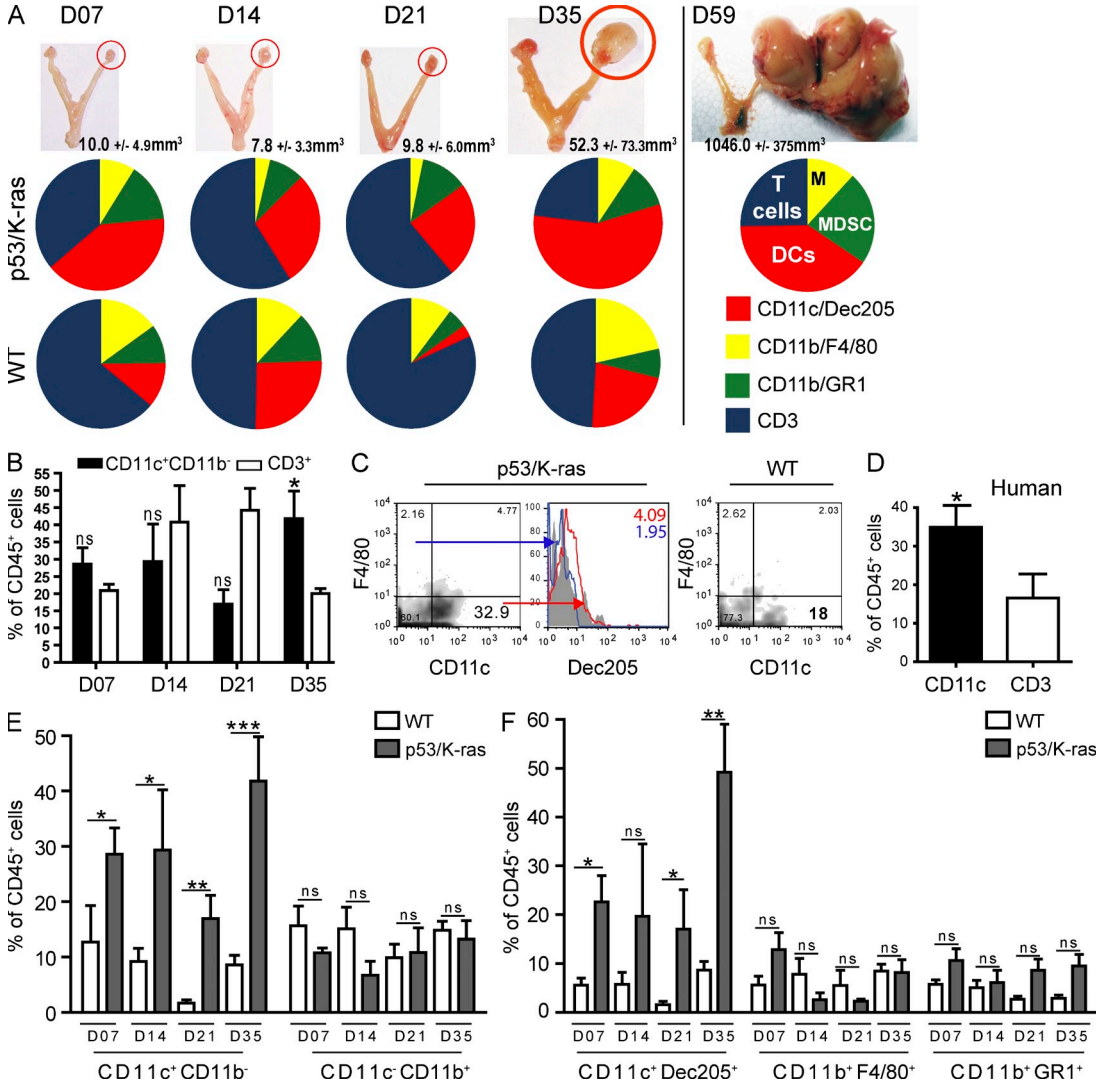

Figure 4. A change in the inflammatory microenvironment converges with the exponential growth of p53/K-ras tumors. (A) Top, images of explanted reproductive organs from p53/K-ras mice after receiving adenovirus. Middle and bottom, quantified flow analysis of resected tumors (red circle; primordial and advanced) from p53/K-ras (middle; $n = 4–6$) and WT (bottom; $n = 6–8$) animals, which received adenovirus previously. Slices represent mean percentages of CD45⁺ leukocytic infiltrates. (B) Comparative analysis of CD45⁺CD11c⁺CD11b⁻ and CD45⁺CD3⁺ cells infiltrating tumors of p53/K-ras mice at the indicated time points ($n = 4–8$). (C) Density plots of p53/K-ras tumors or WT ovaries which received adenovirus 35 d before (gated on CD45⁺ cells). Histogram of CD45⁺F4/80⁺CD11c⁻ (blue) and CD45⁺CD11c⁺F4/80⁻ (red). Numbers in the right corner are respective mean fluorescence intensity (MFI). (D) Percentage of CD45⁺CD11c⁺ and CD45⁺CD3⁺ cells found within stage III/IV human ovarian carcinoma ($n = 7$). (E and F) Quantification of flow analysis at the indicated time points of ovaries from p53/K-ras ($n = 4–6$) or WT ($n = 6–8$) mice after adenovirus injection. Error bars, SEM. *, $P < 0.05$; **, $P < 0.001$; ***, $P < 0.0001$; ns, no significance).

this stage did not significantly differ from surgically treated ovaries in WT mice, and they were characterized by predominant T cell infiltrates after day 7 (Fig. 4, A [bottom] and B).

Approximately 35 d after adenoviral challenge, coinciding with a change in the ratio of T cells versus DCs (Fig. 4, A and B), palpable tumors become apparent. At this time, these leukocytes show predominant phenotypic determinants of the DC lineage, as they express DEC205 and CD11c (Fig. 4 C) as well as MHC-II. In contrast, these leukocytes did not express the macrophage marker F4/80 (Fig. 4 C) and still lacked expression of the myeloid marker CD11b (Fig. 4 E). We also found comparable ratios of CD11c leukocytes to T cells in advanced human tumor specimens (Fig. 4 D). From this critical turning point at ∼28 d, tumors started growing aggressively, and mice needed to be sacrificed at ∼60 d (Fig. 4 A). Notably, inflammatory infiltrates during this exponential phase predominantly expanded by accumulating CD11c⁺ cells, which outnumbered lymphocytes and remained the most abundant leukocytic subset until terminal stages (Fig. 4, A [middle], E, and F). This dramatic change in infiltrating leukocytes was not observed in WT animals, which were similarly treated with adenovirus-Cre, and is therefore not a result of viral clearance or resolution of inflammation (Fig. 4, A [bottom], E, and F). Therefore, inducible p53/K-ras–dependent ovarian cancer progresses

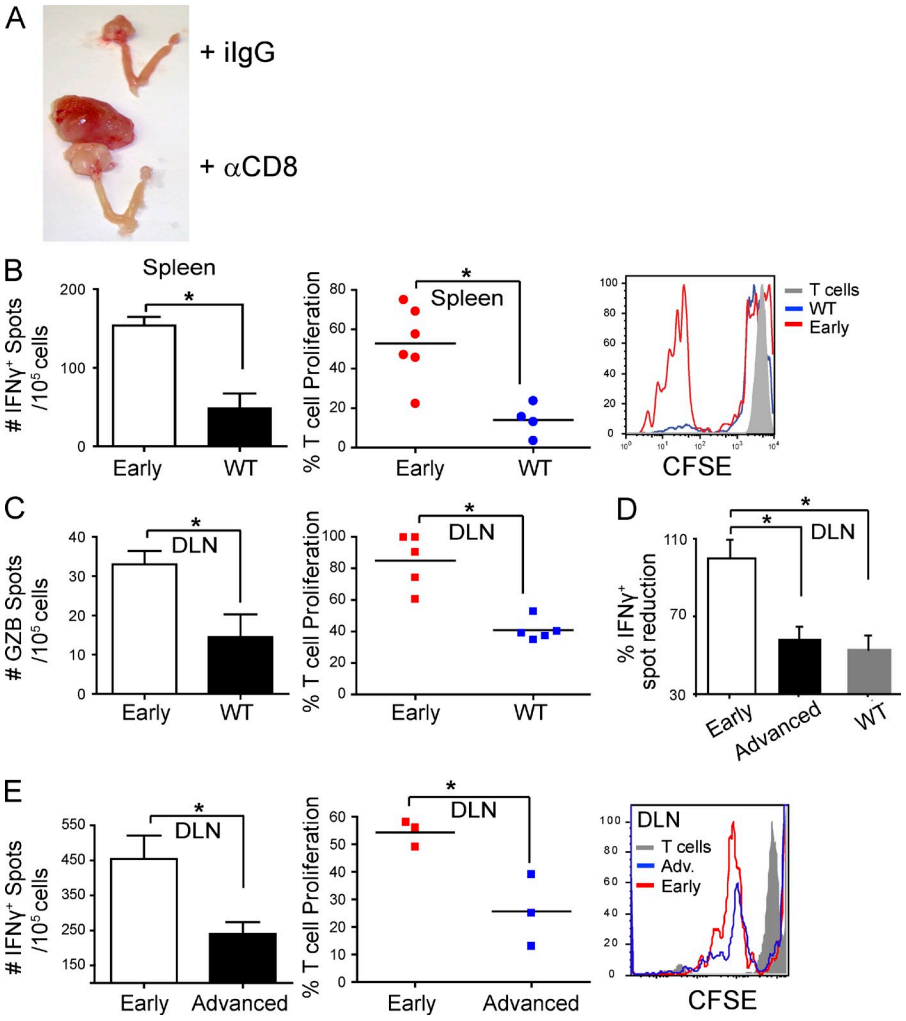

Figure 5. Reduced adaptive immunity during accelerated tumor growth. (A) Representative images of differential tumor burden (primary plus metastatic growth) in mice challenged with intrabursal adenovirus-Cre that received depleting anti-CD8 (α-CD8) versus isotype control (iIgG) antibodies at days −2, 5, 12, and 19 (n = 4/group). (B) Left, ELISPOT analysis of IFN-γ produced by FACS-sorted $CD45^+CD11b^-CD11c^-SSC^{low}CD8_\beta^+/CD4^+$ T cell splenocytes incubated with tumor pulsed BMDCs (10:1). Spleens are from either WT or p53/K-ras (early) animals that received adenovirus-Cre intrabursally 7 d before (n = 5 mice/group; two independent experiments). Middle, quantified proliferation of sorted T cell splenocytes from early tumor-bearing p53/K-ras or WT animals in response to BMDC-presented tumor antigens ($n \geq 5$ mice/group; two independent experiments). Right, representative histogram of CFSE dilution in this experiment. (C) Left, ELISPOT analysis of Granzyme B (GZB) produced by $CD45^+CD11b^-CD11c^-SSC^{low}CD8_\beta^+/CD4^+$ T cells FACS sorted from DLNs (renal) from the same mice, after incubation with tumor pulsed BMDCs (10:1). Middle, quantified proliferation of these lymphatic T cells in response to BMDC-presented tumor antigens. (D) Percentage of IFN-γ spots produced by $CD45^+CD11b^-CD11c^-SSC^{low}CD8_\beta^+/CD4^+$ T cells sorted from the DLN of either WT mice that received adenovirus 7 d before, or p53/K-ras advanced tumor-bearing mice. Normalized to the number of spots produced by sorted DLN T cells from day 7 (early) tumor-bearing mice, which is considered 100% ($n \geq 4$ mice/group; pooled from two independent experiments). (E) Left, ELISPOT analysis of IFN-γ produced by $CD45^+CD11b^-CD11c^-SSC^{low}CD8_\beta^+/CD4^+$ T cells sorted from the DLN of p53/K-ras animals that received adenovirus-Cre intrabursally either 7 d (early) or >50 d (advanced) before. Middle, quantified proliferation of sorted T cells from the same mice in response to BMDC-presented tumor antigens (n = 3 mice/group; three independent experiments, total). Right, representative histogram of CFSE dilution in this experiment. Error bars, SEM. *, $P < 0.05$. Data points on scatter plots represent individual donors for spleens and experimental replicates for pooled DLN. Horizontal bars, SEM. Two independent experiments for all, unless otherwise specified.

through a state of equilibrium that keeps tumor expansion in check for the first 4 wk, followed by a phase of aggressive growth that coincides with a dramatic switch in the signature of tumor-infiltrating leukocytes.

Early anti-tumor immunity is abrogated during aggressive malignant expansion

Notably, antibody-mediated depletion of $CD8^+$ T cells dramatically accelerated aggressive malignant expansion and enhanced tumor burden compared with control mice, which did not develop any extra-ovarian masses at this temporal point and grew smaller primary tumors (Fig. 5 A). Tumor progression in our model therefore both supports and illustrates the cancer immunoediting hypothesis, whereby tumor growth can be controlled by the immune system until tumor cells escape, producing symptomatic cancers (Dunn et al., 2002; Koebel et al., 2007). To identify whether primordial tumor lesions truly elicit specific immune responses, we performed ELISPOT analysis with T cells sorted from mice developing early tumors. As early as at day 7 of tumor progression, sorted splenic T cells specifically reacted to tumor antigen presented by immunocompetent DCs by proliferating and secreting IFN-γ (Fig. 5 B, left). Importantly, these responses were specific for tumor antigens and not the adenovirus because they were absent or significantly diminished when T cells were sorted from WT (non–tumor-bearing) mice identically inoculated with intrabursal adenovirus-Cre (Fig. 5 B). Differential tumor-specific responses indicative of cytolytic T cells (Granzyme B ELISPOT analysis) were also observed between WT and transgenic mice using T cells sorted from DLNs (renal; Fig. 5 C), with corresponding differences in proliferation in response to tumor antigens (Fig. 5 C) and IFN-γ ELISPOT analysis (Fig. 5 D). Importantly, these data indicate that advanced tumors remain immunogenic because all lysates used were from late tumors (early tumors are microscopic). In these experiments, T cells

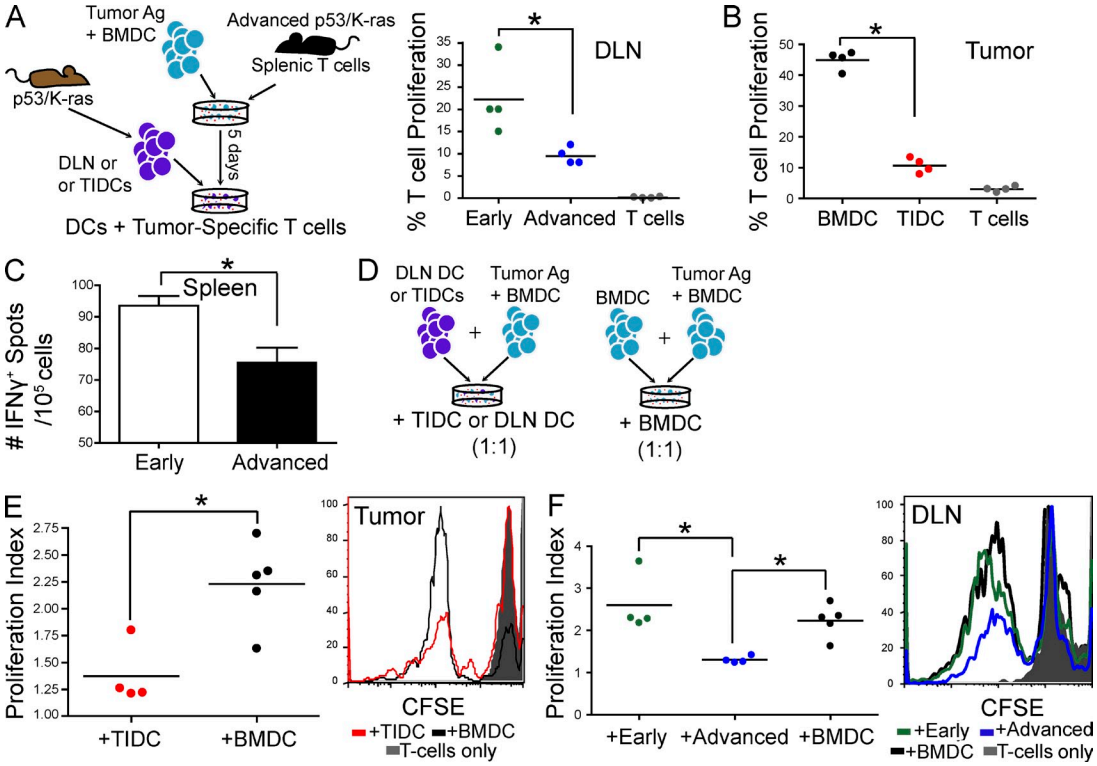

Figure 6. Tumor-resident DCs are transformed from immunostimulatory to immunosuppressive during tumor progression. (A) Left, $CD3^+$ T cells were obtained from spleens of advanced tumor-bearing p53/K-ras animals, and then added to cultures containing BMDCs (10:1) which were previously pulsed with lysed tumor cells. 5 d later, sorted (nonpulsed) $CD45^+CD11c^+$ DCs from the DLNs or tumors (tumor-infiltrating DCs; TIDCs) were co-cultured with the tumor-specific $CD3^+$ T cells, after CFSE labeling (10:1). Right, percentage of proliferated T cells which were cultured with sorted DCs from the DLN of mice with advanced tumors or animals with primordial tumors (early; received adenovirus 7 d before) or DCs from advanced tumors (B). (C) ELISPOT analysis of the responses induced by $CD45^+CD11c^+$ DCs, sorted from the spleens of early and advanced tumor-bearing mice, and directly incubated with tumor-reactive T cells, obtained as in A. (D) Tumor-specific $CD3^+$ T cells were obtained as in A, and then added to culture wells, which contained tumor pulsed BMDCs (1:1). Either sorted $CD45^+CD11c^+CD11b^{+/-}$ DCs or unpulsed BMDCs were added to these cultures making a 1:1:1 ratio (T cell/pulsed BMDC/sorted DC/BMDC). (E) Left, proliferation indices of T cells in response to the addition of tumor infiltrating DCs (TIDCs) or BMDCs. Right, representative histogram of CFSE dye dilution. (F) Left, proliferation indices of T cells in response to the addition of BMDCs or DLN DCs sorted from mice with early or advanced tumors. Right, representative histogram of CFSE dilution. $n = 4$ mice/group. BMDC cultures were done in quad- or quintuplicate. Even stronger differences were obtained using all tumor-pulsed BMDCs (not depicted). Error bars, SEM. Data points on scatter plots represent experimental replicates for pooled DLN or tumors. Horizontal bars, SEM. *, $P < 0.05$. Representative of at least two independent experiments in all panels ($n = 3$–4 mice/group).

sorted from early tumor-bearing mice reacted against BMDCs pulsed with lysates of tumor cells derived from advanced (>60 d) specimens. However, T cells sorted from the DLNs of advanced (>50 d) tumor-bearing mice produced significantly fewer IFN-γ spots in response to the same antigens (Fig. 5, D and E, left). T cell unresponsiveness at advanced stages was further confirmed by diminished proliferative responses in response to the same tumor antigens (Fig. 5 E, middle and right). Because DCs pulsed with cells derived from advanced tumors induced significant proliferative responses in early tumor-associated T cells, these data demonstrate that tumor-specific T cells become intrinsically less responsive during advanced malignant progression. Therefore, T cell–dependent tumor-specific immune responses are elicited from a very early stage after tumor initiation, but they are abrogated during the course of the disease.

Immunostimulatory antigen-presenting cells in primordial tumor lesions are replaced by immunosuppressive DCs in advanced ovarian cancer

The cancer immunoediting hypothesis has recently evolved to include a role for tumor-induced immunosuppression in accelerated tumor growth (Schreiber et al., 2011). However, the relative contribution of specific tolerogenic mechanisms in individual tumors remains unknown. To determine how phenotypic changes in tumor microenvironmental leukocytes drive the transition from equilibrium to accelerated tumor growth and influence anti-tumor T cell unresponsiveness, we first analyzed the immunostimulatory potential of $CD11c^+$ DCs sorted from the DLNs of primordial (day 7) tumor lesions (Fig. 6 A). In agreement with the quantifiable anti-tumor immunity taking place at this time, we found that DCs from early tumor-bearing mice, in the absence of exogenous antigen, induced measurable expansion in tumor-reactive T cells taken from

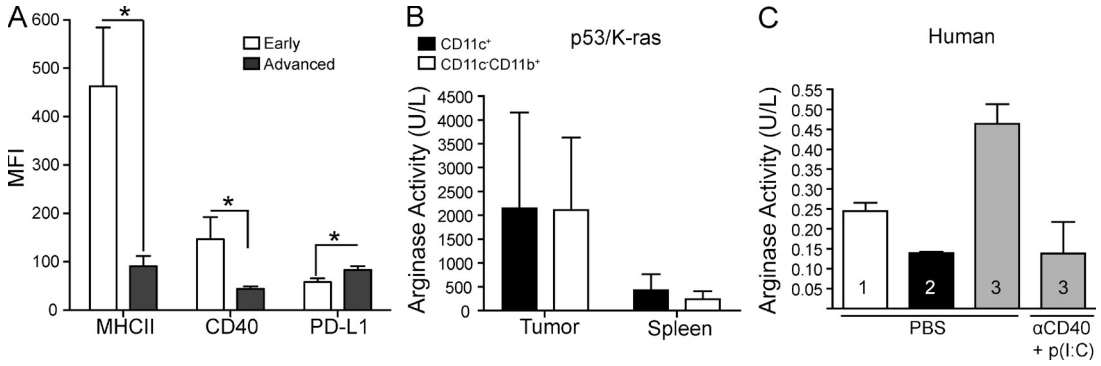

Figure 7. Tumor-infiltrating DCs exhibit a tolerogenic phenotype. (A) Mean fluorescent intensity (MFI) of CD40, MHCII, and PD-L1 on $CD45^+CD11c^+$ DCs from early (ovaries 7 d after adenovirus injection) or advanced tumor masses (n = 4/group). (B) Arginase activity of $CD45^+CD11c^+$ cells sorted from advanced dissociated tumors and spleens of p53/K-ras animals (performed in quadruplets). (C) $CD45^+CD14^-CD20^-CD3^-CD11c^+Dec205^+$ cells from three separate advanced human tumors cultured with PBS or αCD40 and poly(I:C) for 24 h. Experiments were performed in duplicate. Error bars, SEM. *, $P < 0.05$. Representatives of two independent experiments are shown.

animals with advanced tumors, and therefore are overtly immunostimulatory (Fig. 6 A). In contrast, DCs sorted from the DLNs of advanced tumors (Fig. 6 A), or dissociated tumor masses (Fig. 6 B) of advanced tumors, induced minimal proliferative T cell responses. Decreased immunostimulatory activity was further identified in splenic DCs sorted from advanced tumor-bearing mice, compared with mice challenged only 7 d earlier in more sensitive ELISPOT analysis (Fig. 6 C).

We then sought to define how early and advanced tumor microenvironmental DCs influence the capacity of other leukocytes to drive anti-tumor immunity. Remarkably, DCs sorted from dissociated advanced tumors suppressed tumor-specific proliferation induced by immunocompetent DCs (Fig. 6, D and E). We again found that $CD11c^+$ DCs sorted from advanced tumor DLNs elicited comparable immunosuppressive activity in multiple experiments (Fig. 6 F). In contrast, DCs derived from the DLNs of nascent tumor lesions did not impair at all the strong expansion of tumor-reactive T cells elicited by tumor-pulsed BMDCs (Fig. 6 F). Together, these data indicate that DCs in the microenvironment of nascent tumor lesions are actively presenting tumor antigens to anti-tumor T cells, which corresponds with measurable anti-tumor immunity. In contrast, after tumors have started undergoing exponential growth, tumor microenvironmental DCs are not only incapable of inducing significant protective immune responses but they also become overtly immunosuppressive.

Phenotypically distinct DCs drive both immunosurveillance and immunological escape during ovarian cancer progression

Corresponding to the differential immunostimulatory capacity of DCs during tumor initiation and escape, we found significantly lower levels of activating MHCII and CD40 on DCs from advanced stages of tumor growth (Fig. 7 A). Providing a foundation for the additional immunosuppressive activity of DCs from exponentially growing tumors, we identified that they expressed higher levels of tolerogenic PDL-1, compared with DCs in macroscopically undetectable primordial tumor lesions and their DLNs (Fig. 7 A). Most importantly, we also identified strong (immunosuppressive) Arginase activity in $CD11c^+$ DCs sorted from advanced solid tumors, which was comparable to their $CD11b^+CD11c^-$ macrophage/MDSC counterparts but not in splenic leukocytes (Fig. 7 B). Additionally, we detected high levels of Arginase activity in $CD45^+CD14^-CD20^-CD3^-CD11c^+DEC205^+$ DCs sorted from three separate advanced human tumors, which could be reduced by incubation with synergistic immunostimulatory agonists (Fig. 7 C). Therefore, decreased expression of co-stimulatory mediators and a mixture of immunosuppressive mechanisms converge in DCs from advanced tumors to abrogate protective immunity.

Together, our data thus far reveal an opposing function for tumor-associated DCs during the equilibrium versus the escape phase of tumor progression. To define to what extent phenotypically different DCs truly control tumor progression, we first brought double (p53/K-ras) transgenic mice to a B6 background. That resulted in slightly delayed tumor progression (80 vs. 60 d until terminal disease), although tumors still developed with 100% penetrance. Syngeneic transgenic mice were then reconstituted with the BM of CD11c-DTR ITGAX mice, which allows selective temporary ablation of the DC compartment through the administration of diphtheria toxin (Jung et al., 2002; Zammit et al., 2005). As expected, depletion resulted in significantly lower proportions of ovarian resident $CD11c^+$ DCs (Fig. 8 A) within 24 h, compared with chimeric mice which received PBS. Notably, $CD11c^+$ DC depletion immediately before tumor challenge accelerated tumor development, because ∼75% of mice receiving diphtheria toxin grew palpable tumors within 35 d, compared with only ∼25% control mice (Fig. 8 B). Furthermore, a single DC depletion 7 d after tumor challenge, when immunostimulatory DCs promote T cell–mediated anti-tumor immunity, resulted in a dramatic acceleration of tumor progression (Fig. 8, C [top] and D).

In striking contrast, when $CD11c^+$ DCs were depleted at the beginning of the escape phase (∼31 d after adenoviral challenge in this background), elimination of DCs had the opposite effect and retarded tumor progression, as 100% of depleted animals had slower growing, smaller tumors (Fig. 8, C

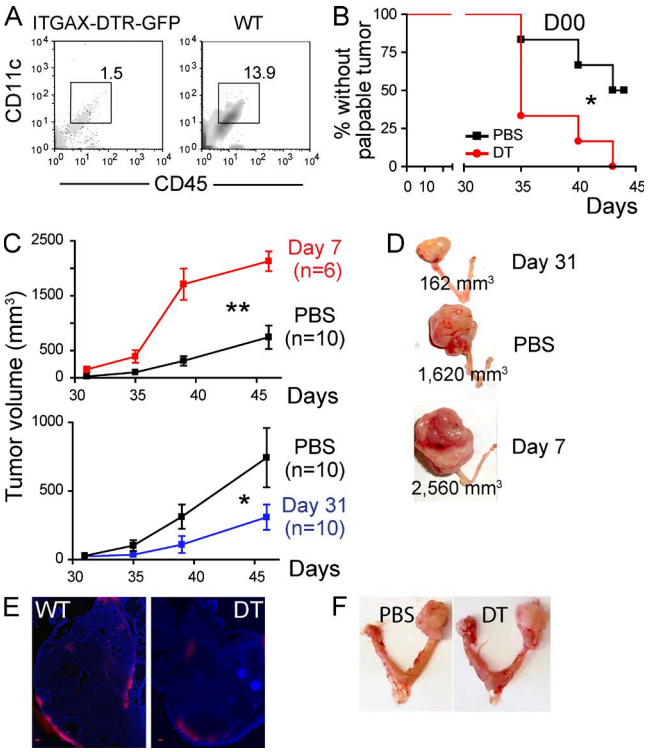

Figure 8. Distinct populations of DCs promote immunosurveillance and the escape phase of tumor development. (A) FACS analysis of dissociated ovaries from mice reconstituted with ITGAX-DTR-GFP or WT BM, 24 h after the i.p. administration of 6 ng/kg of diphtheria toxin. (B) Proportion of p53/K-ras mice reconstituted with BM from ITGAX-DTR-GFP mice without palpable tumors at the indicated times after administration of 6 ng/g of diphtheria toxin (DT) or PBS, 1 d before adenoviral injection (n = 6mice/group). (C) p53/K-ras mice were reconstituted with BM from ITGAX-DTR-GFP mice, and DCs were depleted with one dose of 6 ng/kg of diphtheria toxin (DT) at days 7 (n = 6 mice/group, top), or 31 (n = 10/group, bottom; two pooled independent experiments) after intrabursal adenovirus-Cre. PBS (n = 10/group; two pooled independent experiments) was administered to control mice. (D) Representative size of advanced ovarian tumors in mice depleted of DCs at early versus advanced stages, compared with the absence of DC depletion (PBS). Error bars, SEM. *, $P < 0.05$; **, $P < 0.01$. (E) ITGAX-DTR (DT) or WT mice (n = 3/group) were inoculated intrabursally with 2.5×10^7 plaque-forming units of adenovirus expressing Red-Cherry, and red fluorescence was detected 4 d later. ITGAX-DTR mice received diphtheria toxin (6 ng/g body weight) 24 h before surgery. Brightness, contrast and color balance were uniformly adjusted in whole individual images. Bars, 100 µm. (F) Day 50 tumor growth in p53/Kras mice challenged with adenovirus-Cre and receiving i.p. PBS or diphtheria toxin (DT) 7 d later. Shown are representatives of four mice/group.

[bottom] and D). These effects can only be attributed to phenotypic differences in DCs from different stages of tumor progression because adenoviral transduction was equally effective in both the absence and presence of DCs (Fig. 8 E). In addition, diphtheria toxin had no apparent effect on tumor progression, as we had previously shown in transplantable systems (Fig. 8 F; Huarte et al., 2008a). Together, these results confirm that DCs recruited to ovarian cancer locations are functionally different at different phases of malignant progression and sufficient to drive both initial immunological control of tumor growth and accelerated tumor expansion after equilibrium is broken.

Tumor cell–derived PGE2 and TGF-β1 promote the immunosuppressive activity of immunocompetent DCs

To gain some insight about microenvironmental signals promoting the immunosuppressive activity of potentially immunocompetent DCs, we quantified an array of cytokines and chemokines in media conditioned by cultured tumor cells derived from advanced tumors (UPK10 cells). We identified that immunosuppressive PGE2 and TGF-β1, as well as IL-6, were secreted by tumor cells at very high levels, and their production could be at least partially neutralized with specific antibodies (Fig. 9 A). Notably, both tumor-derived PGE2 and mature TGF-β1 induced the up-regulation of PD-L1 in (immunocompetent) splenic DCs sorted from day 7 tumor-bearing mice because their blockade in tumor-conditioned media prevented PD-L1 overexpression (Fig. 9 B). Most importantly, tumor-conditioned media promoted the immunosuppressive activity of splenic DCs from early tumor-bearing mice, which significantly impaired the strong proliferation of tumor-reactive T cells in response to tumor antigen presented by BMDCs (Fig. 9 C). Tumor-promoted immunosuppressive activity required both PGE2 and mature TGF-β1 because when either was neutralized in the tumor-conditioned media, splenic DCs were incapable of suppressing T cell expansion (Fig. 9 C). Together, these results indicate that immunosuppressive mediators secreted by tumor cells transform potentially immunocompetent DCs into immunosuppressive cells. This transformation, which enables the suppression of anti-tumor T cell–mediated responses, is in part mediated by PGE2 and TGF-β1.

DISCUSSION

Here we have characterized the dynamics of anti-tumor immunity against a new genetic model of inducible ovarian cancer that recapitulates the immune microenvironment of human tumors. We found that ovarian cancer progresses through a prolonged period of controlled tumor growth, in which control involves the recruitment of immunostimulatory DCs that induce measurable T cell–mediated anti-tumor immunity as early as 7 d after tumor challenge. Coinciding with the expansion of DCs with different (immunosuppressive) activity in the tumor microenvironment, tumors abrogate protective immunity and start growing in an aggressive manner. Correspondingly, depletion of DCs, depending on the stage of tumor progression, accelerates tumor progression (early depletion) or inhibits exponential tumor growth (late depletion).

Previous experimental and clinical evidence shows that tumor growth can be kept in check for relatively long periods until tumor cells become edited and escape immune control, growing into clinically obvious cancers (Koebel et al., 2007; Schreiber et al., 2011). Eventual escape from anti-tumor immune surveillance in clinically symptomatic cancers can be

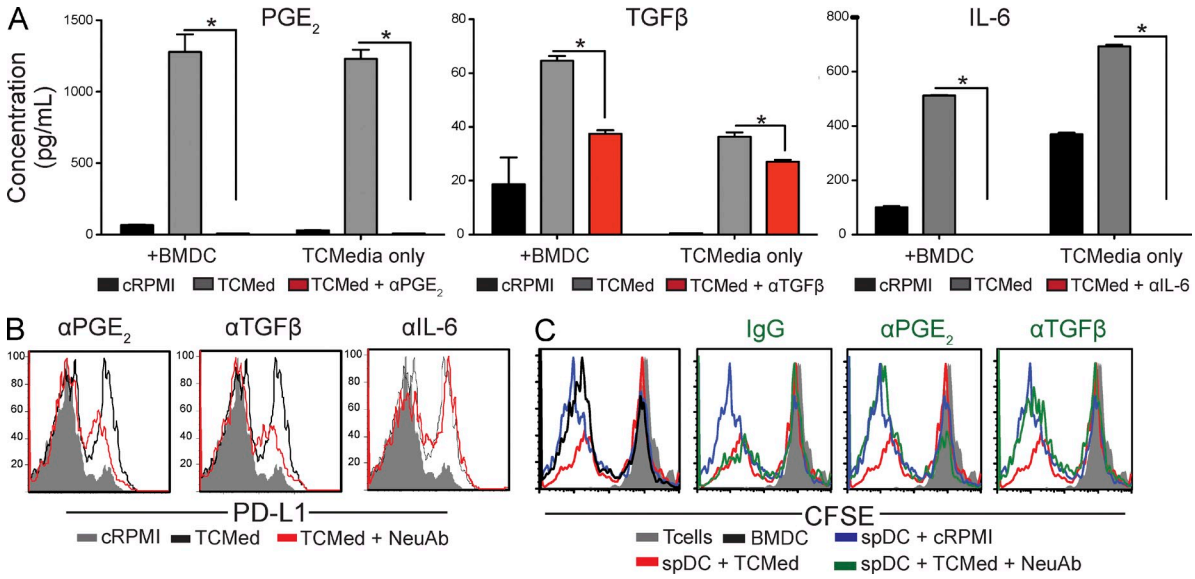

Figure 9. Tumor cell–derived PGE2 and TGF-β1 promote the immunosuppressive activity of DCs. (A) Quantification of PGE2, mature TGF-β1, and IL-6 in media conditioned by tumor cells from advanced (~60 d) ovarian cancer specimens, in the presence or the absence of specific neutralizing antibodies. +BMDCs, BMDCs were incubated for 2 d in tumor-conditioned media before cytokine quantification; cRPMI, RPMI control media; TCmedia, tumor-conditioned media plus an irrelevant IgG; TCmedia+NeuAb, tumor-conditioned media plus specific neutralizing antibodies. Error bars, SEM. *, $P < 0.05$. (B) PD-L1 expression in splenic $CD45^+CD11c^+MHC\text{-}II^+$ DCs sorted from mice carrying early (day 7) tumor lesions, cultured with control versus tumor-conditioned media, in the presence or the absence of specific neutralizing antibodies. (C) Splenic DCs (spDCs) sorted from early tumor-bearing mice were cultured for 48 h in RPMI or tumor-conditioned media (TCMed), in the presence of neutralizing anti-PGE2 or anti–TGF-β1 antibodies (NeuAb), or an irrelevant IgG. These cultured DCs were then incubated with tumor-pulsed BMDCs plus CFSE-labeled tumor-reactive T cells, obtained as in Fig. 6 A (1:1:1 ratio). Unpulsed BMDCs were added to control wells. The panel shows representative histograms of the proliferation of tumor-reactive T cells under different conditions. Representatives of two independent experiments are shown.

attributed to various complementary mechanisms. Originally, the cancer immunoediting hypothesis proposed the progressive loss of immunogenicity by tumor cells as the fundamental driver of accelerated tumor growth. This implies that tumor immunogenicity is primarily sculpted by plastic tumor cells evolving to lose recognizable epitopes. More recently, the model has evolved to include tumor-induced immunosuppression as a contributor to this process, but the importance of individual tolerogenic mechanisms in different tumors remains unclear (Schreiber et al., 2011). Our results show that both equilibrium and exponential ovarian cancer growth are driven independently by the presence of phenotypically dissimilar DCs in the tumor microenvironment. Advanced tumors remain immunogenic because they induce significant proliferative responses in T cells from early tumors. However, the capacity of tumor-specific T cells to react against the same antigen was diminished at advanced stages, which supports previous observations in transplantable models (Nagaraj et al., 2007). Concomitantly, DCs at draining lymphatic and tumor sites are transformed during tumor progression into a cell type that not only presents antigens ineffectively but also actively suppresses T cell responses. Most importantly, protective responses could be restored by depleting this immunosuppressive component, which is distinctively recruited during the phase when tumors spontaneously escape immune control. Such depletion prevents accelerated tumor growth without any direct intervention on the tumor cell. Although we cannot exclude that tumor-associated DCs also promote other important tumorigenic mechanisms (e.g., angiogenesis), our study uncovers the recruitment of immunosuppressive DCs, rather than loss of immunogenicity, as the principal mechanism driving the transition from equilibrium to expansive progression in ovarian cancer. In addition, our data provide a mechanistic rationale for targeting regulatory DCs as the characteristic product of the pathological myelopoiesis orchestrated by advanced ovarian cancers.

Importantly, similar to tumor development in adult humans, our model develops in healthy adult mice without active mutations during embryonic development. We found that breaking equilibrium between tumor growth and immune control to achieve aggressive tumor growth is significantly challenging in this context and is indicated by the necessity of two simultaneous mutation events for malignancy. In any case, despite the importance of p53, our work supports previous studies which demonstrate that its homozygous ablation does not immediately result in any obvious phenotype, and tumors require >7 mo to advance even after the addition of a second mutation, different from *KRAS* (Flesken-Nikitin et al., 2003). Overall, our results suggest that even if primordial tumor lesions can be established, tumor microenvironmental leukocytes prevent their unrelenting growth for a relatively prolonged equilibrium phase. Only when the inflammatory

infiltrate undergoes precise phenotypic and quantitative changes does tumor growth become exponential and thus clinically apparent.

MATERIALS AND METHODS

Animals and tissues. WT C57BL/6 mice were procured from the National Cancer Institute or The Jackson Laboratory, under Institutional Animal Care and Use Committee approval. Stage III–IV human ovarian carcinoma specimens were procured through Research Pathology Services at Dartmouth-Hitchcock Medical Center under institutional approval (CPHS17702). Single cell suspensions or cDNA were generated as we previously described (Huarte et al., 2008b). The primary mouse cell line, UPK10, was generated by culturing a mechanically dissociated B6 LSL-K-ras$^{G12D/+}$p53$^{loxP/loxP}$ primary ovarian tumor mass. Tumor cells were passaged a total of 10× and lead to terminal tumor masses 28 d after i.p. injection in WT animals. HOSEpiC are epithelial cells from healthy ovaries cryopreserved either at primary or passage one cultures (ScienCell Research).

Generation of transgenic mice. To generate the LSL-K-ras$^{G12D/+}$p53$^{loxP/loxP}$ model, we used Kras^{tm4Tyj} and Trp53^{tm1Brn} mice (Jackson et al., 2001; Jonkers et al., 2001), obtained from the NCI Mouse Models of Human Cancers Consortium. For the indicated experiments, mice were brought to a C57BL/6 background.

Chimera generation and antibody-mediated depletion. BM cells (10×10^6) isolated from ITGAX DTR-GFP mice were injected intravenously into B6 K-ras$^{G12D/+}$p53$^{loxP/loxP}$ after undergoing lethal doses of gamma irradiation, as we previously described (Huarte et al., 2008a). Mice were checked for complete reconstitution by identifying GFP$^+$CD45$^+$CD11c$^+$ cells in peripheral blood ~6 wk after reconstitution. ITGAX-DTR (DT) or WT mice (n = 3/group) were inoculated intrabursally with 2.5×10^7 plaque-forming units of adenovirus expressing Red-Cherry (Gene Transfer Vector Core, University of Iowa).

CD8 T cells were depleted through intraperitoneal administration of rat anti–mouse CD8 antibodies (clone# YTS 169.4; BioXCell), 2 d before intrabursal administration of 500 µg adenovirus-Cre. Injections were repeated at days 5, 12, and 19 (250 µg each). Control mice received a rat IgG2b isotype control (clone# LTF-2; BioXCell).

Proliferation and suppression assays. For T cell proliferation assays, day 7 BMDCs, generated as previously described (Scarlett et al., 2009), were cultured overnight with either freeze-thawed lysed UPK10 or dissociated primary tumors. BMDCs were added to cultures of CFSE (Invitrogen)-labeled T cells at a 10:1 ratio and were analyzed 3 d later by flow cytometry. For DC proliferation assays (Fig. 6 A, schematic), Pan T cell isolation (Miltenyi Biotec) was performed using spleens taken from p53/K-ras animals with advanced (>50 d after AdvCre injection) tumors. CD3$^+$ T cells were then cultured for ~4–5 d with tumor-pulsed BMDCs as described at a 10:1 ratio to generate tumor-specific T cells. Tumor-specific T cells were then CFSE labeled and added to V-bottom 96-well plates which contained sorted DCs (10:1 ratio). Cultures were analyzed by flow cytometry 5 d later. For the suppression assay (Fig. 6 C, schematic), tumor-pulsed BMDCs were added to CFSE-labeled tumor-specific T cells (1:1), followed by addition of unpulsed BMDCs or sorted DCs (1:1:1 ratio) in V-bottom 96-well plates. Analyses were performed 3 d later.

Neutralization assays. PGE2 (Cayman Chemical) and mature TGF-β1 and IL-6 (both eBioscience) were quantified by ELISA in media conditioned for 2 d by >90% confluent UPK10 tumor cells. When indicated, neutralizing antibodies against mouse PGE2 (7 µg/ml; 2B5; Cayman Chemical), TGF-β1 (5 µg/ml; 2Ar2; Abcam) or IL-6 (4 µg/ml; PeproTech) were added to the media. Goat anti–mouse IgG (Jackson ImmunoResearch Laboratories, Inc.) was used as a control.

Histological analysis. For frozen tissue, organs of mice were collected and embedded in Tissue-Tek OCT. For paraffin-embedded tissue, organs were fixed in 4% formaldehyde overnight at 4°C. Fixed sections (8 µm) were then made from frozen or paraffin-embedded tissue blocks. For analysis of tumor histological type, pan Cytokeratin (AE1+AE3) 1:50 dilution, smooth muscle actin (SMA; EP184E) 1:500 dilution, Desmin (Y266) 1:500 dilution, Cytokeratin 8 (ab59400) 1:250 dilution, and Vimentin (RB202) 1:200 dilution were purchased from Abcam and immunohistochemical analyses were performed by the Dartmouth Pathology Translational Research Core (Lebanon, NH). For immunohistochemistry of leukocytes, tissues were blocked using α-CD32, followed by staining with anti–mouse biotinylated CD45 (104), MHCII (M5/114.15.2), or APC-conjugated Dec205 (NLDC-145; all obtained from BioLegend). Completion of immunohistochemical procedure was performed according to the manufacturer's instructions (Vector Laboratories). Slides were then viewed at various magnifications using a fluorescence microscope (Nikon) and the NIS-Element Imaging software.

Flow cytometry. Flow cytometry was performed on a FACSCanto (BD). Sorting was performed on a FACSAria sorter (BD). Anti–mouse antibodies: CD45 (30-F11), CD11b (M1/70), DEC205 (NLDC-145), F4/80 (BM8), GR1 (RB6-8C5), CD3 (145-2C11), CD8β (YTS156.7.7), CD8α (53–6.7), CD4 (GK1.5), CD25 (PC61.5), and PDL-1 (10F.9G2; all obtained from BioLegend); and Foxp3 (FJK-16s), CD11c (N418), and MHC-II (NIMR-4; eBioscience). Anti–human antibodies: CD45 (H130), DEC205 (HD30), CD11c (3.9), CD3 (OKT3), CD11b (ICRF44), HLA-DR (L243), CD14 (HCD14), and CD20 (2H7; all obtained from BioLegend). The purity of FACS-sorted populations was >90%.

Quantitative real-time PCR and sequencing. Messenger RNA copy number of various loci was assessed by quantitative real-time PCR using an Real Time PCR Machine (Applied Biosystems). Primers for RT-PCR experiments to detect human K-ras expression using SYBR green: Kras forward, 5′-TGTGGACGAATATGATCCAACAA-3′; and Kras reverse, 5′-TCCTCATGTACTGGTCCCTCATT-3′. Primers for mouse and human GAPDH expression using TaqMan: GAPDH forward, 5′-CCTGCACCACCAACTGCTTA-3′; GAPDH reverse, 5′-AGTGATGGCATGGACTGTGCT-3′; and probe (FAM/TAMRA), 5′-CCTGGCCAAGGTCATCCATGACAACTTT-3′.

Cytokine/chemokine detection. Sorted tumor-associated cells from either p53/K-ras mice or Stage III–IV human ovarian carcinoma specimens were stimulated for 4 h with 50 ng PMA/1 µg/ml ionomycin in complete RPMI containing 10% FBS. Supernatants were used for cytokines and chemokines using a human or mouse Custom-Plex panel cytokine assay (Bio-Rad Laboratories), according to the manufacturer's instructions.

Arginase activity assay. Cells from either p53/K-ras mice (tumor and spleens) or Stage III–IV human ovarian carcinoma specimens were sorted. Quantitative colorimetric arginase determination was performed using an Arginase Activity detection kit (BioAssay Systems). In brief, $0.05–0.25 \times 10^6$ cells were washed and lysed for 10 min in 50 µl of 10 mM Tris-HCl, pH 7.4, containing 0.15 mM pepstatin A, 0.2 mM leupeptin, and 0.4% (vol/vol) Triton X-100. Supernatants from lysates were then used to complete the assay according to the manufacturer's instructions. For human analysis, we cultured cells with agonistic CP-870,893 αCD40 monoclonal antibody and poly (I:C) as previously described (Scarlett et al., 2009). We obtained the CP-870,893 monoclonal antibody from Pfizer.

ELISPOT. Total or sorted cells were obtained from dissociated spleens, renal DLNs, or tumors of p53/K-ras or WT controls. T cells were then co-cultured for 72 h in coated and blocked ELISPOT plates, in a 10:1 ratio among day 7 BMDC or sorted DC, which were previously pulsed (4 h) with freeze-thawed lysed UPK10 cells or resected primary tumor (10 DC/1 tumor cell). All cultures were maintained in complete RPMI containing 10% FBS. Analysis was then continued according to manufacturer's protocol (IFN-γ, eBioscience; and Granzyme B, R&D Systems).

Immunoblotting. TRIzol reagent (Invitrogen) was used to obtain protein from either stage III or IV human solid tumor specimens. In brief, frozen tissues were cut into tiny pieces, and then added to complete RPMI where they were further macerated using the end of a syringe's plunger. The dissociated tissues were spun and the pellets were added to TRIzol, and the completion

of the protein extraction was performed according to the manufacturer's instruction. Proteins were diluted in 7 µl Laemmli buffer, boiled, loaded onto a 12% Ready Gel Tris-HCL gel (Bio-Rad Laboratories), transferred to a nitrocellulose membrane, blocked, and incubated with the indicated primary Ab. Immunoreactive bands were developed using horseradish peroxidase–conjugated secondary Abs (Bio-Rad Laboratories) and chemiluminescent substrate (GE Healthcare). Human KRAS, β-actin, and β-tubulin were detected using a mouse anti–human mAb (clone no. ab55391), rabbit anti–human (ab8227), and goat anti–human (ab21057) antibodies, respectively (all from Abcam).

Statistical analyses. Differences between the means of experimental groups were analyzed using the Mann-Whitney or the χ^2 test. Survival was analyzed with the Log-rank test, both using Prism 4.0 software (GraphPad Software). Proliferation indices, defined as the mean number of cell divisions that the responding cells underwent, were calculated using FlowJo software (Tree Star).

We thank C. Hart and R. O'Meara from the Research Pathology at Dartmouth-Hitchcock Medical Center; J. Gorham and K.A. Muirhead from the Dartmouse Facility for bringing our floxed p53 mouse to a B6 mouse through speed congenics; the Microscopy, Flow Cytometry, Genomics, and Animal Facilities at The Wistar Institute, particularly Jamie Hayden, Fred Keeney, and Jeffrey Faust; and Diana Martinez for her exceptional technical support.

This study was supported by a Liz-Tilberis Award; NCI Grants R01CA124515, R01CA124515S, R01CA157664, U54CA151662, P30CA10815, and R21CA132026; and DoD grant OC100059. U.K. Scarlett was supported by the National Research Service Award F31CA134188.

The authors declare no competing financial interests.

Submitted: 11 July 2011
Accepted: 23 January 2012

REFERENCES

Bell, D., A. Berchuck, M. Birrer, J. Chien, D.W. Cramer, F. Dao, R. Dhir, P. Disaia, H. Gabra, P. Glenn, et al; Cancer Genome Atlas Research Network. 2011. Integrated genomic analyses of ovarian carcinoma. *Nature*. 474:609–615. http://dx.doi.org/10.1038/nature10166

Bernardini, M.Q., T. Baba, P.S. Lee, J.C. Barnett, G.P. Sfakianos, A.A. Secord, S.K. Murphy, E. Iversen, J.R. Marks, and A. Berchuck. 2010. Expression signatures of TP53 mutations in serous ovarian cancers. *BMC Cancer*. 10:237. http://dx.doi.org/10.1186/1471-2407-10-237

Clark, C.E., S.R. Hingorani, R. Mick, C. Combs, D.A. Tuveson, and R.H. Vonderheide. 2007. Dynamics of the immune reaction to pancreatic cancer from inception to invasion. *Cancer Res*. 67:9518–9527. http://dx.doi.org/10.1158/0008-5472.CAN-07-0175

Connolly, D.C., R. Bao, A.Y. Nikitin, K.C. Stephens, T.W. Poole, X. Hua, S.S. Harris, B.C. Vanderhyden, and T.C. Hamilton. 2003. Female mice chimeric for expression of the simian virus 40 TAg under control of the MISIIR promoter develop epithelial ovarian cancer. *Cancer Res*. 63:1389–1397.

Dinulescu, D.M., T.A. Ince, B.J. Quade, S.A. Shafer, D. Crowley, and T. Jacks. 2005. Role of K-ras and Pten in the development of mouse models of endometriosis and endometrioid ovarian cancer. *Nat. Med*. 11:63–70. http://dx.doi.org/10.1038/nm1173

Dunn, G.P., A.T. Bruce, H. Ikeda, L.J. Old, and R.D. Schreiber. 2002. Cancer immunoediting: from immunosurveillance to tumor escape. *Nat. Immunol*. 3:991–998. http://dx.doi.org/10.1038/ni1102-991

Flesken-Nikitin, A., K.C. Choi, J.P. Eng, E.N. Shmidt, and A.Y. Nikitin. 2003. Induction of carcinogenesis by concurrent inactivation of p53 and Rb1 in the mouse ovarian surface epithelium. *Cancer Res*. 63:3459–3463.

Hamanishi, J., M. Mandai, M. Iwasaki, T. Okazaki, Y. Tanaka, K. Yamaguchi, T. Higuchi, H. Yagi, K. Takakura, N. Minato, et al. 2007. Programmed cell death 1 ligand 1 and tumor-infiltrating CD8+ T lymphocytes are prognostic factors of human ovarian cancer. *Proc. Natl. Acad. Sci. USA*. 104:3360–3365. http://dx.doi.org/10.1073/pnas.0611533104

Huarte, E., J.R. Cubillos-Ruiz, Y.C. Nesbeth, U.K. Scarlett, D.G. Martinez, R.J. Buckanovich, F. Benencia, R.V. Stan, T. Keler, P. Sarobe, et al. 2008a. Depletion of dendritic cells delays ovarian cancer progression by boosting antitumor immunity. *Cancer Res*. 68:7684–7691. http://dx.doi.org/10.1158/0008-5472.CAN-08-1167

Huarte, E., J.R. Cubillos-Ruiz, Y.C. Nesbeth, U.K. Scarlett, D.G. Martinez, X.A. Engle, W.F. Rigby, P.A. Pioli, P.M. Guyre, and J.R. Conejo-Garcia. 2008b. PILAR is a novel modulator of human T-cell expansion. *Blood*. 112:1259–1268. http://dx.doi.org/10.1182/blood-2007-12-130773

Jackson, E.L., N. Willis, K. Mercer, R.T. Bronson, D. Crowley, R. Montoya, T. Jacks, and D.A. Tuveson. 2001. Analysis of lung tumor initiation and progression using conditional expression of oncogenic K-ras. *Genes Dev*. 15:3243–3248. http://dx.doi.org/10.1101/gad.943001

Jemal, A., R. Siegel, E. Ward, Y. Hao, J. Xu, and M.J. Thun. 2009. Cancer statistics, 2009. *CA Cancer J. Clin*. 59:225–249. http://dx.doi.org/10.3322/caac.20006

Jonkers, J., R. Meuwissen, H. van der Gulden, H. Peterse, M. van der Valk, and A. Berns. 2001. Synergistic tumor suppressor activity of BRCA2 and p53 in a conditional mouse model for breast cancer. *Nat. Genet*. 29:418–425. http://dx.doi.org/10.1038/ng747

Jung, S., D. Unutmaz, P. Wong, G. Sano, K. De los Santos, T. Sparwasser, S. Wu, S. Vuthoori, K. Ko, F. Zavala, et al. 2002. In vivo depletion of CD11c+ dendritic cells abrogates priming of CD8+ T cells by exogenous cell-associated antigens. *Immunity*. 17:211–220. http://dx.doi.org/10.1016/S1074-7613(02)00365-5

Koebel, C.M., W. Vermi, J.B. Swann, N. Zerafa, S.J. Rodig, L.J. Old, M.J. Smyth, and R.D. Schreiber. 2007. Adaptive immunity maintains occult cancer in an equilibrium state. *Nature*. 450:903–907. http://dx.doi.org/10.1038/nature06309

Kurman, R.J., and IeM. Shih. 2011. Molecular pathogenesis and extraovarian origin of epithelial ovarian cancer—shifting the paradigm. *Hum. Pathol*. 42:918–931. http://dx.doi.org/10.1016/j.humpath.2011.03.003

Nagaraj, S., and D.I. Gabrilovich. 2010. Myeloid-derived suppressor cells in human cancer. *Cancer J*. 16:348–353. http://dx.doi.org/10.1097/PPO.0b013e3181eb3358

Nagaraj, S., K. Gupta, V. Pisarev, L. Kinarsky, S. Sherman, L. Kang, D.L. Herber, J. Schneck, and D.I. Gabrilovich. 2007. Altered recognition of antigen is a mechanism of CD8+ T cell tolerance in cancer. *Nat. Med*. 13:828–835. http://dx.doi.org/10.1038/nm1609

Sato, E., S.H. Olson, J. Ahn, B. Bundy, H. Nishikawa, F. Qian, A.A. Jungbluth, D. Frosina, S. Gnjatic, C. Ambrosone, et al. 2005. Intraepithelial CD8+ tumor-infiltrating lymphocytes and a high CD8+/regulatory T cell ratio are associated with favorable prognosis in ovarian cancer. *Proc. Natl. Acad. Sci. USA*. 102:18538–18543. http://dx.doi.org/10.1073/pnas.0509182102

Scarlett, U.K., J.R. Cubillos-Ruiz, Y.C. Nesbeth, D.G. Martinez, X. Engle, A.T. Gewirtz, C.L. Ahonen, and J.R. Conejo-Garcia. 2009. In situ stimulation of CD40 and Toll-like receptor 3 transforms ovarian cancer-infiltrating dendritic cells from immunosuppressive to immunostimulatory cells. *Cancer Res*. 69:7329–7337. http://dx.doi.org/10.1158/0008-5472.CAN-09-0835

Schreiber, R.D., L.J. Old, and M.J. Smyth. 2011. Cancer immunoediting: integrating immunity's roles in cancer suppression and promotion. *Science*. 331:1565–1570. http://dx.doi.org/10.1126/science.1203486

Wang, Y., R. Wu, K.R. Cho, K.A. Shedden, T.J. Barder, and D.M. Lubman. 2006. Classification of cancer cell lines using an automated two-dimensional liquid mapping method with hierarchical clustering techniques. *Mol. Cell. Proteomics*. 5:43–52.

Wilke, C.M., I. Kryczek, and W. Zou. 2011. Antigen-presenting cell (APC) subsets in ovarian cancer. *Int. Rev. Immunol*. 30:120–126. http://dx.doi.org/10.3109/08830185.2011.567362

Xing, D., G. Scangas, M. Nitta, L. He, X. Xu, Y.J. Ioffe, P.J. Aspuria, C.Y. Hedvat, M.L. Anderson, E. Oliva, et al. 2009. A role for BRCA1 in uterine leiomyosarcoma. *Cancer Res*. 69:8231–8235. http://dx.doi.org/10.1158/0008-5472.CAN-09-2543

Zammit, D.J., L.S. Cauley, Q.M. Pham, and L. Lefrançois. 2005. Dendritic cells maximize the memory CD8 T cell response to infection. *Immunity*. 22:561–570. http://dx.doi.org/10.1016/j.immuni.2005.03.005

Zhang, L., J.R. Conejo-Garcia, D. Katsaros, P.A. Gimotty, M. Massobrio, G. Regnani, A. Makrigiannakis, H. Gray, K. Schlienger, M.N. Liebman, et al. 2003. Intratumoral T cells, recurrence, and survival in epithelial ovarian cancer. *N. Engl. J. Med*. 348:203–213. http://dx.doi.org/10.1056/NEJMoa020177